Nat. Hazards Earth Syst. Sci. Discuss., 2, 7225–7267, 2014
www.nat-hazards-earth-syst-sci-discuss.net/2/7225/2014/
doi:10.5194/nhessd-2-7225-2014
© Author(s) 2014. CC Attribution 3.0 License.

Natural Hazards and Earth System Sciences
Open Access
Discussions

This discussion paper is/has been under review for the journal Natural Hazards and Earth System Sciences (NHESS). Please refer to the corresponding final paper in NHESS if available.

Internal structure of event layers preserved on the Andaman Sea continental shelf, Thailand: tsunami vs. storm and flash flood deposits

D. Sakuna-Schwartz[1,*], P. Feldens[1], K. Schwarzer[1], S. Khokiattiwong[2], and K. Stattegger[1]

[1]Institute of Geosciences, Kiel University, Otto-Hahn-Platz 1, 24118 Kiel, Germany
[2]Oceanography Unit, Phuket Marine Biological Center, P.O. Box 60, 83000 Phuket, Thailand
[*]now at: Oceanography Unit, Phuket Marine Biological Center, P.O. Box 60, 83000 Phuket, Thailand

Received: 10 September 2014 – Accepted: 29 October 2014 – Published: 1 December 2014

Correspondence to: D. Sakuna-Schwartz (daroonwans@gmail.com)

Published by Copernicus Publications on behalf of the European Geosciences Union.

Abstract

Tsunami, storm and flash event layers, which have been deposited over the last century on the shelf offshore from Khao Lak (Thailand, Andaman Sea), are identified in sediment cores based on sedimentary structures, grain size compositions, Ti / Ca ratios and ^{210}Pb activity. Individual offshore tsunami deposits are 12 to 30 cm in thickness and originate from the 2004 Indian Ocean tsunami. They are characterized by (1) the appearance of sand layers enriched in shells and shell debris, (2) cross lamination and (3) the appearance of rip-up clasts. Storm deposits found in core depths between 5 and 82 cm could be attributed to individual storm events by using ^{210}Pb dating in conjunction with historical data of typhoons and tropical storms and could thus be securely differentiated from tsunami deposits. Massive sand layers enriched in shells and shell debris characterize the storm deposits. The last classified type of event layer represents flash floods, which is characterized by a fining-upward sequence of muddy sediment. The most distinct difference between the storm and tsunami deposits is the lack of rip-up clasts, mud, and terrigenous material within the storm deposits. Terrigenous material transported offshore during the tsunami backwash is therefore an important indicator to distinguish between offshore storm and tsunami deposits.

1 Introduction

Tsunami waves propagating into shallow waters as well as related backwash flows can erode, transport and deposit significant amounts of sediments in the inner shelf environment (e.g. Paris et al., 2010; Goto et al., 2011), here defined as 0 to 30 m water depth. The behaviour of tsunami waves is controlled by the source earthquake or landslide and the ocean basin's morphology on a larger scale, as well as by the inner-shelf and coastal bathymetry and probably the hydrological conditions on a local scale (Cheng and Weiss, 2013; Spiske et al., 2013; Goto et al., 2014). Coastal and inner shelf bathymetry is the most important factor controlling backwash flow (Le Roux and

NHESSD

2, 7225–7267, 2014

Vargas, 2005; Paris et al., 2010; Feldens et al., 2012; Spiske et al., 2014). The structure and texture of tsunami deposits in offshore areas mainly depends on the local sediment sources, the geomorphology of the seafloor, the tsunami wave height and the number of waves if more than one wave hits the shoreline during the run-up and backwash (Sakuna et al., 2012). Both the bathymetry and available sediments are highly variable in shallow marine environments (e.g. Dartnell and Gardner, 2004). A complex composition of offshore tsunami deposits is therefore expected, with potentially quick changes both in space and time (Shanmugam, 2012). A tsunami's impact in deeper waters may be preserved within sediments below the storm wave base (e.g. Weiss and Bahlburg, 2006; Weiss, 2008). However, while the tsunami's impact increases with decreasing water depth towards the coastline, only very few offshore tsunami deposits have been reported until now.

Research on offshore tsunami deposits has to consider the low preservation potential of tsunami deposits in shallow waters due to reworking and transport by waves (Weiss and Bahlburg, 2006), tides and bioturbation (Wheatcroft and Drake, 2003). Reworking is intensified in areas with low accumulation rates, where tsunami deposits cannot quickly escape the surface mixing layer. Therefore, it is not surprising that the described offshore deposits of historical tsunami – not considering inferred tsunami palaeorecords on geological timescales (Cantalamessa and Celma, 2005; Le Roux and Vargas, 2005; Fujiwara and Kamataki, 2007; Spiske et al., 2014) – are highly variable in thickness, texture and structure (e.g. van den Bergh et al., 2003; Abrantes et al., 2008; Goodman-Tchenov et al., 2009; Paris et al., 2010; Smedile et al., 2011; Sakuna et al., 2012; Milkert et al., 2013). Offshore tsunami deposits range from centimetres to 1 m in thickness while spanning grain sizes from mud to boulders, including terrigenous and marine sediments over one or several layers, different fossil assemblages and different sedimentary structures (Sakuna et al., 2012). A further problem is the differentiation between storm and tsunami deposits, which has been widely discussed for deposits left on land (e.g. Nott, 2003; Goff et al., 2004; Kortekaas and Dawson, 2007; Morton et al., 2007; Switzer and Jones, 2008; Lario et al., 2010; Phantuwongraj and

NHESSD
2, 7225–7267, 2014

Choowong, 2011; Lorang, 2011; Richmond et al., 2011; Ramírez-Herrera et al., 2012; Brill et al., 2014b), but no reliable sedimentological criteria have yet been developed to distinguish offshore storm deposits from tsunami deposits. Generally, shallow-water, proximal tempestites are characterized by basal erosional contacts and a sequence from normal gradation to cross stratification to plane lamination, with frequently preserved ripples at the top (Einsele et al., 1991; Allison et al., 2005). However, not all tempestites comprise all these features. Furthermore, in monsoon-dominated areas, flash flood deposits occur frequently (Kale, 2003; Malmon et al., 2004) and have to be considered while identifying offshore backflow tsunami deposits. Flash floods can comprise a large percentage of a river's yearly discharge and can form hyperpycnal flows due to high suspended sand and mud concentrations (Mulder et al., 2003; Bourrin et al., 2008), which have been established for tsunami backwash flows (Le Roux and Vargas, 2005). Directly in front of river mouths or ephemeral streams, flash flood deposits are typically coarse grained (Postma, 2001) or comprise alternating sand and mud layers (Martin, 2000). However, they also comprise stratified deposits of silty clays at more remote locations (Cutter and Diaz, 2000). The Andaman Sea (Thailand) is an area where all these types of event deposits can be studied. It has been subjected to a few strong storms over the last decades, regularly impacted by the northeast and southwest monsoons, with the latter accompanied by flash floods, and hit by the 2004 Indian Ocean tsunami. Based on a collection of six sediment cores from the Andaman Sea, the objectives of this study are to (a) identify, describe and discuss the tsunami, storm and flash flood deposits in sediment cores and to (b) identify proxies that can be used to distinguish tsunami, storm and flash flood deposits from each other.

2 Regional setting

The investigation area near Pakarang Cape is located on the western side of the southern Thai-Malay peninsula offshore from Phang Nga province (Fig. 1). The Ayeyarwady–Salween river system is the main source supplying fine-grained sediment

NHESSD
2, 7225–7267, 2014

into the Andaman Sea (Rodolfo, 1969; Colin et al., 1999), which is highly seasonal, with more than 80 % of the annual discharge during the SW monsoon (Ramaswamy et al., 2004). The majority of the Andaman Basin is classified as sediment starved (Rodolfo, 1969; Panchang et al., 2008; Schwab et al., 2012). The coastline north and south of Pakarang Cape represents an embayed coast with sandy beaches commonly separated by rocky headlands. In general, the shelf gently dips offshore, reaching 60 m water depths within a distance of 30 km from the coastline. Pakarang Cape itself is surrounded by a 3 km long reef platform (Goto et al., 2007; Choowong et al., 2009; Di Geronimo et al., 2009). The tides in this area are mixed semidiurnal, with most days having two high tides and two low tides. The mean tidal range extends from 1.1 m during neap tide to 3.6 m during spring tide (Thampanya et al., 2006). Based on geomorphological evidence from sandy hooks and spits, northward-directed current-induced longshore sediment transport occurs in the study area (Choowong et al., 2009; Brill et al., 2014a). Maps of the nearshore bathymetry and sediment distribution have been created following the 2004 Indian Ocean tsunami (e.g. Di Geronimo et al., 2009; Feldens et al., 2009, 2012), but the maps cover only a small percentage of the Andaman Sea shelf. According to these studies, mud patches are widespread in water depths between 5 and 15 m north and south of Pakarang Cape. Several granite outcrops are scattered along the inner shelf at water depths of 5–10 m and on the mid-shelf at a water depth of approximately 30 m. Extensive cassiterite mining both on- and offshore has affected the area over the last century (Hylleberg et al., 1985; Usiriprisan et al., 1987). Offshore, visible remnants of the mining activities include up to 7 m deep holes at water depths of 20–25 m NW of Pakarang Cape (Feldens et al., 2009).

The climate of this region is influenced by the tropical monsoon, with the northeast monsoon lasting from December to February, causing dry weather conditions, and the southwest monsoon lasting from May to September, bringing strong westerly winds and heavy rainfall (Khokiattiwong et al., 1991). While no studies on flash floods have been published for the Andaman Coast, they are expected to occur regularly during the southwest monsoon and have been reported by the local population. Strong storm

NHESSD
2, 7225–7267, 2014

events are rare in this area (Jankaew et al., 2008; Brill et al., 2011), and only nine strong storm events were recorded within a 180-nautical-mile radius of Phuket between 1945 and 1996 (Table 1).

The coastal area of the Andaman Sea was seriously affected by the 2004 Indian Ocean tsunami (Chavanich et al., 2005; Siripong, 2006; Szczuciński et al., 2006; Choowong et al., 2007; Goto et al., 2007; Umitsu et al., 2007). Since then, several studies (Di Geronimo et al., 2009; Sugawara et al., 2009; Feldens et al., 2009, 2012) have focussed on the tsunami's impact on the shelf area offshore from Khao Lak. Only minor influence and a few deposits related to the 2004 tsunami could be found 3 to 5 years later offshore between 5 and 70 m water depths (Di Geronimo et al., 2009; Sugawara et al., 2009; Feldens et al., 2012; Sakuna et al., 2012; Milker et al., 2013). Due to the reworking of shelf sediments (Sakuna et al., 2012) and the re-establishment of the coastline (Choowong et al., 2009; Grzelak et al., 2009) following the tsunami, the remaining offshore tsunami deposits have been chiefly found in locally sheltered positions adjacent to granitic outcrops, within an incised channel system and in areas of locally higher sediment accumulation rates (Feldens et al., 2012; Sakuna et al., 2012; Milker et al., 2013).

3 Methods

During three research cruises in December 2007, December 2008 and February/March 2010, side-scan sonar data were obtained using a Klein 595 side-scan sonar (384 kHz) and a Benthos 1624 side-scan sonar (100 and 400 kHz). The side-scan sonars were towed behind the vessel with approximately 10 to 50 m offset from the GPS antenna. This offset was accounted for by a constant value for each profile when calculating the position of the tow fish. Side-scan sonar data were recorded in digital format employing the Isis software package (Triton Elics Int.). These data were processed and geo-referenced using the same software to create side-scan sonar mosaics of the study area. In this study, areas of higher backscatter are displayed with

NHESSD
2, 7225–7267, 2014

darker colours. A total of 60 gravity cores using a Ruhmor-type gravity corer (8 cm diameter) were collected (see Fig. 1) based on the on-site interpretation of the side-scan sonar and previous shallow seismic mapping (Feldens et al., 2009, 2012). Gravity cores could only be retrieved from fine-grained (silt and finer) seafloor sediments, as the corer could not penetrate into seafloor composed of sand. In all the cores, the sediment–water interface was preserved. Out of the 60 cores that have been taken, 6 are presented in this study (Fig. 1, Table 2). The sediment slabs were radiographed to detect internal sedimentary structures and unconformities. The grain size composition was determined every 1 cm with a laser-based particle sizer device with a measuring range of 0.04 to 2000 µm. Therefore, grains larger than 2000 µm were separated prior to the measurements. The statistical parameters of the grain size distributions were calculated in phi (Φ) units with $\Phi = -\log_2 d$ (d being the grain size in mm) (Krumbein, 1938) using the logarithmic method of moments available with the GRADISTAT software (Blott and Pye, 2001). Measurements of ^{210}Pb activity were done for two sediment cores (030310-C3 and 050310-C4) to assess the sediment accumulation rates. The sediment samples were dried, ground and analysed using gamma spectrometry at the Leibniz-Laboratory for Radiometric Dating and Isotope Research, Kiel, Germany. As the ^{137}Cs activity was mostly below the detection limits, these data were not used for further analysis. The sediment accumulation rates presented in this study serve only as an approximation and were assessed from the decline in the excess ^{210}Pb activity following the equations used by Robins and Edington (1975) and McKee et al. (1983).

$$\mathrm{SAR} = \lambda \times z \times [\ln(A_0/A_z)]^{-1}, \quad (1)$$

where λ is the decay constant (= 0.0311 year^{-1}), z is the depth in the core (cm), A_0 is the specific activity of excess ^{210}Pb at a particular reference horizon (Bq kg^{-1}) and A_z is the specific activity of excess ^{210}Pb at depth z below the reference horizon (Bq kg^{-1}).

NHESSD
2, 7225–7267, 2014

4 Results

4.1 Subsurface sediment sequence

The description of the sediment sequence in the sediment cores is based on X-radiographic images. If not mentioned otherwise, the depth values in the following section refer to core depths. The core positions are indicated in Fig. 1. An overview of all the available core details is given in Fig. 2, while the side-scan sonar data showing the sediment distribution from the areas where the cores have been taken are shown in Fig. 3. The sedimentary features and the interpretation of all the studied cores are summarized in Table 3 and Fig. 5. In general, four different facies are recognized within the presented cores. Most frequently occurring are layers composed of mainly clayey silt with a few sand layers, which are commonly laminated and generally fining upward with transitional boundaries (individual laminae could not be sampled). Bioturbation is rarely observed in this facies. Furthermore, sand layers that are partly massive and show slight lamination occur. Shells are scattered throughout the sand layers. At the top, rippled shapes draped with mud are partly preserved. In several cores, several-centimetres-thick layers comprised of shells and shell debris with variable fraction of coarse sand and gravel exist. Finally, poorly sorted sediment units comprising mud to sand and including mud clasts are found.

4.1.1 Core 030310-C3 (Fig. 2)

Core 030310-C3 (97 cm in length) was collected 3.2 km offshore at a water depth of 9.5 m, approximately 100 m west of a granitic outcrop (see Fig. 3a). In the vicinity of the coring position, the backscatter in the side-scan sonar is low, representing silt and fine sand proven by grab samples and grain size analyses.

The lowermost 2 cm of the core is composed of massive fine-grained sediment. At 95 cm, an erosional contact with laminated sediments exists. These laminated sediments extend up to 82 cm (Table 3a-V). The laminations are slightly inclined and the

NHESSD
2, 7225–7267, 2014

sediment is fining upward. Traces of bioturbation are not observed. Above a wavy and erosional contact at 82 cm, a massive sand layer including few shells extends up to 79 cm (Table 3a-IV). The upper boundary of the sand layer is sharp. Above, fining-upward laminated mud extends from 79 to 69 cm. No traces of bioturbation are observed here either. Notably, a large sand clast can be observed from 77 to 73 cm in this core section. Laminations bend around the base of this clast and onlap at both sides. At 70 cm, a sharp contact separates the laminated mud from a massive sand layer that extends up to 67 cm (Table 3a-III). While half of its upper boundary appears transitional, this is likely related to disturbance (smearing) during the sampling procedure. Above 67 cm, laminated sediment prevails up to 56 cm. Interbedded sand layers at 66 cm, from 63 to 62 cm and from 61 to 60 cm show preserved ripple structures, each forming a sharp upper contact. At 56 cm, an erosive unconformity separates the laminated material from a 9 cm thick sand layer. While the lower 4 cm of this sand layer appears massive, clear cross lamination is observed within its upper 5 cm up to 47 cm (Table 3a-II). No shells or bioturbation traces can be observed in the sand layer. At 47 cm, an irregular and erosional contact exists. Above, laminated sediment is present from 47 to 36 cm. In this interval, a massive sand layer, 1 cm in thickness with sharp upper and lower contacts, interbeds at 42 cm. The erosional boundary of the laminated sediment is observed at 36 cm. Mud clasts have been found between 34 and 31 cm (Table 3a-I), with the diameter increasing in the upper layer. Above a transitional boundary, a sand layer rich in shell debris is present between 31 and 29 cm (Table 3a-I). No bioturbation traces are observed within this layer. Above a sharp contact at 29 cm, laminated mud is deposited up to 26 cm. Here, a sand layer 2 cm in thickness is observed above an erosional contact. Its upper, sharp contact at 24 cm is ripple-shaped. Above the contact at 24 cm, laminated material extends up to approximately 6 cm. Single bioturbation traces are observed between 17 and 16 cm core depth. In this interval, no lamination is recognized. Apparently, the deformed features in the upper 13 cm of the core are related to disturbances during coring. A highly irregular boundary from approximately 8 to 6 cm separates the laminated material from more homogeneous sediment that includes a

NHESSD
2, 7225–7267, 2014

few coarser sand grains. Above a sharp boundary at 1 cm, homogeneous fine-grained material is observed.

4.1.2 Core 030310-C2 (Fig. 2)

Core 030310-C2, with a length of 23 cm, was retrieved from silty seafloor at 11.5 m water depth, 3.3 km offshore from the navigational entrance to Thap Lamu harbour (Fig. 1). Due to strong fishing activities with fixed nets, no side-scan sonar surveys could be carried out here.

At the base of this core, between 23 and 17 cm, bioturbated fine sand is observed. Few shells are scattered throughout the layer. A layer composed of coarse sand and gravel, including shells, laterite fragments and coral debris, is separated from the fine sand layer below. A layer composed of muddy fine sand is deposited above, separated by erosional boundaries at 17 cm at the base and at 13 cm at its top (Table 3b-II). Above 13 cm, an 8.5 cm thick layer of muddy fine sand including a few shell fragments is observed. A sharp boundary with an irregular shape – interpreted as a load clast – appears at 4.5 cm (Table 3b-I). At the top of the core, homogeneous silt to fine sand with frequent traces of bioturbation is present.

4.1.3 Core 050310-C4 (Fig. 2)

Core 050310-C4, with a length of 55 cm, was retrieved 6.3 km offshore at a water depth of 15.3 m. The position is located within a patch of silt to fine sand that is surrounded by patches of medium to coarse sand (see Fig. 3c).

Bioturbation traces are recognized in the lowermost 3.5 cm of the core from 55 to 51.5 cm within a silty to sandy material. At 51.5 cm, a layer of coarse sand, 3 cm in thickness, is separated from the sediment above and beneath by sharp erosional contacts. The layer appears massive and small shells are observed (Table 3c-IV). A finer, presumably silty layer is deposited above 48.5 cm. This layer is characterized by the occurrence of a few shells and frequent bioturbation traces. It is separated by a sharp

NHESSD
2, 7225–7267, 2014

contact at 37.5 cm from a 1 cm thick coarse sand layer. Above, a fining-upward sequence of laminated fine-grained sediment is observed from 37.5 to 28.5 cm, but the laminae could not be sampled individually as their thicknesses were too small (from 1 to 5 mm in thickness, Table 3c-III). At 28.5 cm, a sharp but irregular contact – interpreted as load clast – exists. At 24 cm, an erosional contact separates a 7 cm thick layer mainly composed of shells (Table 3c-II). Laminated sediment is found again from 17 to 15 cm. Following a sharp boundary, coarse sediment including shells is deposited above 15 cm (Table 3c-I). Due to disturbances during the sampling procedure in the field, the upper boundary of the layer cannot be clearly recognized. However, based on the abundance of shells, it is likely situated at approximately 2 cm. The upper 2 cm of the core comprises fine-grained sediment with a few bioturbation traces.

4.1.4 Core 030310-C7 (Fig. 2)

Core 030310-C7, with a length of 65 cm, was retrieved from a water depth of 11.9 m, 2.9 km offshore (approximately 4.9 km south of Pakarang Cape) in an area where the seafloor is composed of silty to fine sediment. The boundary between silt- and fine-sand-covered seafloor to coarse sand, gravel and boulders is situated approximately 70 m to the southeast. Granitic outcrops rise approximately 500 m to the east (see Fig. 3d).

At the base of the core, laminated material is fining upward between 65 and 61 cm. At 61 cm, a sharp contact with a 6 cm thick layer composed of coarse sand and occasional gravel exists (Table 3d-VII). However, the layer is not massive and no clear fining-upward or downward trend can be recognized. The layer is draped by a centimetre of muddy material on top. Cross laminations of coarser sediment are identified from light scattering in X-ray images at 54 and 53 cm (Table 3d-VI). A sharp contact has been found at 53 cm that separates a 6 cm thick fining-upward sequence of laminated fine-grained material, which shows no sign of bioturbation traces (Table 3d-V). At 47 cm, an irregular sharp contact separates the laminated sediment from a layer of sand, in which faint indications of cross laminations are observed (Table 3d-IV). At

NHESSD
2, 7225–7267, 2014

the top of the sand layer at 42.5 cm, ripple structures draped by a 0.5 cm thick layer of mud are preserved. Between 42 and 39 cm, a mixture of sand and mud clasts prevails. Above a sharp contact at 39 cm, a 4 cm thick layer comprising coarse sand and pebbles exists. A transitional contact at 35 cm separates a 1 cm thick sand layer from slightly laminated silty fine sediment. A fining-upward sequence of coarse sand, partly pebble-size corals and pebbles exists from 34 to 28 cm (Table 3d-III). Above 28 cm, an 8 cm thick sequence of cross-laminated bedforms is observed with several corals and shells scattered throughout (Table 3d-II). Up to 18 cm, the layer is covered by sand. Above 18 cm, a layer of mixed clasts composed of sand and mud exists, with few shells scattered throughout. Few bioturbation traces are observed at the top of the layer (Table 3d-I).

4.1.5 Core 050310-C2

Core 051207-31, with a length of 70 cm, was retrieved 7.2 km offshore at a water depth of 15.9 m at a boundary of patches that are composed of silt to fine sand and partly coarse sand (Fig. 3e). From sub bottom profiler data, it is known that this position is located in a partly filled incised channel system (Feldens et al., 2012).

At the core-base, laminated fine-grained material exists between 70 and 68 cm (Table 3e-VI). A transitional boundary separates a 2 cm thick layer of massive coarse grains extending from 68 to 66 cm. With transitional lower and upper boundaries, the sediment, mainly composed of muddy sand with a few shells, is fining upwards between 66 and 64 cm. Sediment changes transitionally into a 2.5 cm thick layer of massive coarse sand at approximately 61 cm (Table 3e-V). Above 58.5 cm, the sediment is gradually fining upward. At 53 cm, an erosive contact separates the fining-upward sequence from a 3 cm thick layer comprising pebbles, coarse sand and shell fragments (Table 3e-IV). Laminated material is present above up to 47 cm. A few shells are located within this layer. Following a sharp contact at 47 cm, a coarse, fining-upward sequence is present, capped by a sharp boundary at 45 cm (Table 3e-III). Fining-upward sequences with a sharp boundary composed of pebbles, coarse sand and shell frag-

NHESSD
2, 7225–7267, 2014

ments exist between 41 and 38, 38 and 34.5, 34.5 and 32, 32 and 25, 25 and 20, 20 and 15.5, and 15.5 and 11.5 cm. At 11.5 cm, an erosional contact separates a fining-upward sequence from a layer of shells that forms the upper 10 cm of this core (Table 3e-I).

4.1.6 Core 051207-31

Core 050310-C2, with a length of 75 cm, was collected at a water depth of 9.8 m, located 1.5 km northeast of Pakarang Cape. The seafloor at the sampling position is composed of silt to fine sand (Fig. 3b).

The lower part of the core from 75 to 40 cm comprises a silty matrix with a few corals and abundant shells scattered throughout. Clasts that are a few centimetres in diameter and composed of sand-sized sediment are observed at 72 and 53 cm. A bioturbation trace is found from 63 to 60 cm. Above an erosional contact at 40 cm, a 9 cm thick layer, mainly composed of large shells in a sandy matrix, is observed (Table 3f-III). Above an erosional boundary at 31 cm, laminated mud is observed (Table 3f-II). Between a sharp upper and lower contact, a sand layer in which shells are present extends from 25 to 24 cm. The sand layer is draped by a 1 cm thick layer of fine-grained, laminated sediment. A similar sequence is observed above: a 1 cm thick layer of sand (23 to 22 cm) with a sharp upper and lower boundary is draped by laminated muddy material that reaches up to 14 cm. From 20 to 14 cm, several centimetre-thick clasts composed of sandy material disrupt the laminations (Table 3f-I). Above a sharp contact at 14 cm, a 2 cm thick sequence of likely silty to fine sand material including shell fragments exists. At 12 cm, a 0.5 cm thick homogenous mud layer is draped on the layer beneath. However, it is difficult to determine whether this layer extends along the whole core width, as the left part of the core was disturbed during sampling. Above, a coarser sand layer with a sharp upper contact is deposited from 11.5 to 7.5 cm, which includes pieces of corals and shell fragments. The top of the core (above 7.5 cm core depth) was partly disturbed during sampling, but apparently consists of bioturbated but otherwise homogeneous fine-grained material, with the exception of few sandy clasts with a diameter of 1–5 mm.

NHESSD
2, 7225–7267, 2014

4.2 ^{210}Pb activity and Ti / Ca ratios

The Ti / Ca log ratios in all six cores are stable, with the exception of coarse sediment layers, where Ti / Ca log ratios vary between −2.8 and −0.1 (Fig. 2).

The excess ^{210}Pb activity profile measured in core 030310-C3 (Fig. 4) reveals a general decline of activity with core depth. The activity profile includes intervals of anomalously low activity (e.g. 50 and 68 cm core depth) that correspond to coarser-grained sediments. The average sediment accumulation rate for this core is 1.94 cm yr^{-1}. However, the maximum sediment accumulation rate for the top 20 cm could be as much as 7.5 cm yr^{-1}.

The activity profile of core 050310-C4 (Fig. 4) shows an exponential decrease in the excess ^{210}Pb activity in the sediment above the shell deposit layer in the 19–24 cm core depth range (see Fig. 2 and Table 3c-II). Below 24 cm, the profile approaches the general decline in excess ^{210}Pb activity. The average sediment accumulation rate for the whole core is 0.53 cm yr^{-1}. Using data only from the upper 10 cm, the sedimentation rate is up to 1.73 cm yr^{-1}.

5 Discussion

5.1 Identification of event deposits

The analysed core data allow us to differentiate between three types of event deposits found on the inner shelf offshore from Khao Lak. They are related to (1) flash floods, (2) storms and typhoons, and (3) the 2004 Indian Ocean tsunami.

The majority of the fine-grained, laminated sediments (Figs. 2 and 5 and Table 3) are interpreted as flash flood deposits, which have previously not been described on the Andaman Sea. In general, the most important source from which fine sediment is supplied to accumulate on continental shelves is river discharge (Kuehl et al., 1985; Wright and Nittrouer, 1995; Geyer et al., 2004; Crokett and Nittrouer, 2004; Palinkas et al.,

NHESSD
2, 7225–7267, 2014

2006). River discharge is minor in the investigation area (Jankaew et al., 2008; Feldens et al., 2009; Brill et al., 2011). However, increasing anthropogenic activities during the last century, such as tin mining, construction of tourist resorts, deforestation, agriculture and urbanization, all cause river discharge due to increased exposure weathering and the erosion of fine sediment (Wolanski and Spagnol, 2000). In the course of flash floods during the southwest monsoon (rainy season), these fine sediments will be subsequently transported through ephemeral channels towards the ocean (e.g. Curran et al., 2002; Mulder et al., 2003; Malmon et al., 2004; Owen, 2005). Enhanced sedimentation due to anthropogenic impacts was observed in different settings such as tropical estuaries in Papua New Guinea, Vietnam, Australia and Indonesia (Wolanski and Spagnol, 2000); the Pearl River in Hong Kong (Owen and Lee, 2004; Owen, 2005); and the Waiapu River in New Zealand (Wadman and McNinch, 2008). Offshore from Khao Lak, Feldens et al. (2012) found fine-grained sediments deposited above 15 m water depth that were composed of silt and fine sand and orientated parallel to the shoreline. These fine sediments offshore from Khao Lak, which show little cohesiveness due to a high percentage of coarse silt and fine sand, have been deposited during a multitude of small-scale events (Table 3a-V, 3c-III, 3d-V, 3e-VI and Fig. 5). In the X-ray images, these deposits are recognized as laminated sections of mud, silt and fine sand. Regular reworking and re-deposition from suspension is indicated by the frequent occurrence of fining-upward sequences, showing a lack of bioturbation that may be explained by high accumulation rates, which are expected during flash floods (Wheatcroft et al., 2008). Notable is the frequent occurrence of thin sand layers less than 1 cm in thickness with sharp upper and lower boundaries that are within the laminated core sections in core 051207-31. Based on side-scan sonar images, this core is situated close to a boundary of fine and coarse sediment (Fig. 3). The transport of sand into areas covered by finer sediment in the range of annual cycles without exceptional storm events was demonstrated by repeated side-scan sonar mapping offshore from Khao Lak (Feldens et al., 2012).

NHESSD
2, 7225–7267, 2014

Layers showing parts of the characteristics of proximal tempestites are frequent in the X-ray images (Figs. 2 and 5), including sharp and partly erosional lower contacts, preserved cross laminations, ripples and graded-bedded sand without mud content, which therefore follow the characteristics of proximal tempestites (Einsele, 1991). Storms influence the sedimentary record due to oscillatory water movements caused by waves, with the shear stress imposed on seafloor sediments decreasing with increasing water depth (Weidong et al., 1997; Allison et al., 2005). The Andaman Shelf is seldom affected by severe storms and typhoons (see Table 1), which commonly form in the South China Sea during the northeast monsoon (data compiled by TMD, 2014). Storms lose their energy while crossing the Thai-Malay continent. In contrast, cyclone tracks originating within the Bay of Bengal are predominantly directed towards the coast of India, Bangladesh and Myanmar (Singh et al., 2000). Based on ^{210}Pb activity, several proposed event deposits in the cores 030310-C3 and 050310-C4 have ages of less than 50 years but are older than the 2004 Indian Ocean tsunami. During the time interval from 1945 to 1996, only nine historical tropical storms passed the investigation area (Table 1). Using the estimated accumulation (based on ^{210}Pb dating) rates of 0.54 to 1.9 cm yr^{-1} for the inner continental shelf, the event layers within 47–62 cm depth have ages of 20 to 30 years. Therefore, they are likely related to Typhoon Gay, which hit this area in 1989. Similarly, core depths from 68 to 70 cm depth correspond to Tropical Storm Sally (1972) or Tropical Depression Sarah (1973). Tropical depressions from the 1960s (Harriet, Lucy and Gloria) may correspond to the event layers from 78 to 82 cm. In core 030310-C7, one event layer extends between 42.5 and 45.5 cm, which is separated from the most recent event layer above by a mud drape. While no age control exists, this layer likely resulted from Tropical Storm Forrest (1992) or tropical depression Manny (1993) or Ernie (1996). Several event layers in the upper part of the cores (layers A, B and C, Table 4 and Fig. 5) are different from the event layers beneath, which are attributed to storm events. They show a larger variability, ranging from 10 cm thick shell deposits to muddy deposits including coarse sand grains, laterites and shell debris to mud deposits including clasts of various compositions. Based on

NHESSD
2, 7225–7267, 2014

the sediment accumulation rates in cores 030310-C3 and 050310-C4, the layers are located between sediments that have been deposited within the last few years (Fig. 4). Due to the absence of large storm events, they have been most likely deposited by the 2004 Indian Ocean tsunami. It is assumed that the event layers at similar core depths within the other cores have been deposited during the 2004 Indian Ocean tsunami as well.

5.2 Identification and features of the tsunami facies

Event deposits attributed to the 2004 Indian Ocean tsunami based on ^{210}Pb dating are grouped into three facies (Table 4 and Fig. 5) representing the variable characteristics of offshore tsunami deposits. They are characterized by sand enriched with shells or shell debris (A), cross lamination (B) and massive layers (C).

Except in core 030310-C3, the observed tsunami deposit sequences show sand enriched with shells or shell debris (facies A) at their base. Seafloor dominated by shells, coral rubble and sand is frequent between 15 and 20 m water depth offshore from Khao Lak (Feldens et al., 2012). Therefore, this layer is likely to be eroded during the propagation of tsunami waves from the open ocean to shallow waters. A marine origin of these deposits is also supported by generally lower Ti / Ca ratios in the massive sand layer compared to the surrounding muddy layers (Fig. 2). Foraminifera transfer functions that developed for the suspected tsunami deposits support a transport of facies A material from these water depths (Milker et al., 2013). A depth of approximately 20 m is substantially lower compared to the depths found during previous studies of tsunami impacts based on wave theory and the analysis of microfossils (e.g. Nanayama and Shigeno, 2006; Weiss and Bahlburg, 2006; Weiss, 2008; Uchida et al., 2010). It is unknown whether the local shelf morphology offshore from Khao Lak prohibited the substantial erosion of material from deeper waters or whether the sediments transported onshore from deeper waters were not preserved. As no storm event occurred between the 2004 tsunami and the time of sampling, the latter appears unlikely, sug-

NHESSD
2, 7225–7267, 2014

gesting that the tsunami deposits offshore from Khao Lak are in fact limited to shallow water depths.

Sediments from facies type A are mostly covered by massive deposits commonly including mud or sand clasts (tsunami deposit facies type C); however, an inverted sequence is found in core 030310-C3. Sediments from facies type C are assumed to be created out of a hyperpycnal tsunami backwash flow (Goff et al., 2004; Morton et al., 2007; Goodman-Tchernov et al., 2009; Sakuna et al., 2012). Accordingly, facies type C is frequently found in the uppermost part of the tsunami sequence and includes material transported during the backwash, as shown by foraminifera indications (Milker et al., 2013) and the presence of laterites and grass (Feldens et al., 2012; Sakuna et al., 2012). The Ti / Ca ratios are not noticeably different from the inferred flash floods deposits, which have to originate from onshore. Tsunami facies type C is not observed within all the cores. The absence of backwash deposits in cores 051207-31 and 050310-C2 may be related to subsequent erosion, with flash flood deposits observed directly on top of the tsunami deposits in core 050310-C2 and the tsunami deposits exposed at the seafloor in core 051207-31. Within core C3, an inverted sequence is observed, which may be explained by several waves approaching the coastline.

Intensive cross bedding, only observed within core 030310-C7, characterizes tsunami facies type B, which is located between facies type A and type C. It may be assumed that the cross bedding is related to multiple flow reversals between the run-up and backwash of the three wave trains approaching the coastline during the 2004 tsunami event (e.g. Siripong, 2006). Cross bedding is a common feature for onshore tsunami deposits, where it was widely used to indicate the hydrodynamic regime during the deposition (Dawson et al., 1996; Nanayama et al., 2000; Goff et al., 2001; Bahlburg and Weiss, 2007; Engel and Brückner, 2011).

NHESSD
2, 7225–7267, 2014

5.3 Comparison of tsunami, storm and flash flood facies

On the Andaman Sea shelf, the presence of deposits related to tsunami, tropical storms and annual flash floods during the summer monsoon season allows us to compare the sedimentary signatures of these events at the same offshore location. The distinction of tsunami deposits from those deposited by other high-energy events, such as storms or hurricanes, are still problematic, even for deposits on land (Nanayama et al., 2000; Kortekaas and Dawson, 2007; Morton et al., 2007; Switzer and Jones, 2008; Phantuwongraj and Choowong, 2011). Previous studies proved that a series of proxies must be applied, e.g. the geomorphological setting, sedimentary structures, microfossil assemblages and geochemical components (Goff et al., 2004, 2010; Kortekaas and Dawson, 2007; Morton et al., 2007; RamÍrez-Herrera et al., 2012; Chagué-Goff et al., 2011; Richmond et al., 2011; Sakuna et al., 2012). The different signatures of the identified event deposits have been summarized in Table 5. In particular, the differentiation between tsunami facies type A and storm deposits appears to be problematic. Storms raise water levels due to their low atmospheric pressure and cause coastal flooding (Ogston et al., 2000; Harris and Heap, 2009). Sediment is kept in suspension and deposited with waning energy levels. This results in deposits of graded sand, frequently showing cross bedding. Wave ripple marks draped with mud are frequently only preserved at the top of the storm deposit sequence (Weidong et al., 1997). While a tsunami event may comprise several waves, thus allowing the deposition of several mud drapes, it is expected that later waves erode the previously deposited mud drapes. Distinct lamina of shells and their fragments are common in storm deposits, most likely because of high-frequency waves (Morton et al., 2007), and have also been observed in tsunami deposits offshore from Khao Lak (this study). Therefore, taken by themselves, neither the observed cross-laminated sections nor the presence of sand rich in shells or shell debris is suitable as a proxy to distinguish tsunami and storm deposits. In contrast, rip-up clasts (both mud and sand clasts, facies type C) were previously used to discriminate storm and tsunami deposits (e.g. Morton et al., 2007; Phantuwongraj and

NHESSD
2, 7225–7267, 2014

Choowong, 2011), as were terrestrial components and anthropogenic artefacts. The backwash transports a variety of material from the hinterland towards offshore, and the high-density backwash flows support the formation of clasts (Dawson and Stewart, 2007; Morton et al., 2007; Shanmugam, 2011; RamÍrez-Herrera et al., 2012). In contrast, erosion during storms is focused on the shoreface and the beach (Snedden et al., 1988; Allison et al., 2005); thus, clasts and terrestrial material are expected to appear less frequently within storm deposits. This highlights the importance of material deposited during the tsunami backwash for the identification of past tsunami events. Further proxies using the increased occurrence of terrestrial material for the discrimination of offshore tsunami and storm deposits could be plants, anthropogenic material (for recent events), or geochemical proxies, such as polycyclic aromatic hydrocarbon (PAH) (Tipmanee et al., 2012) or microfossils (Milker at al., 2013). Tsunami backwash deposits have to be differentiated from flash floods, which can also deposit terrigenous material out of hyperpycnal density flows (Mulder et al., 2003; Bourrin et al., 2008). In fact, little difference exists in the Ti / Ca ratios between flash flood and tsunami deposits offshore from Pakarang Cape. However, flash floods differ from the identified tsunami deposits sedimentologically: they are generally better sorted than tsunami deposits and include less sand, likely relating to the higher energy of the tsunami backwash flow. The higher energy of the backwash flow is further reflected by the generally sharp and erosional boundaries of the backwash deposits, while flash flood deposits show transitional boundaries. Additionally, mud clasts are absent in the observed flash flood deposits. However, no major river outlets exist close to the investigation area, with flash floods flowing into the ocean through a number of ephemeral channels. It is suggested that channelized flash flood deposits are more difficult to distinguish from tsunami deposits.

NHESSD
2, 7225–7267, 2014

6 Conclusions

On the Andaman Sea continental shelf, tsunami, storm and flash flood deposits have been preserved in close vicinity to each other, allowing us to compare their sedimentological characteristics. Flash flood deposits comprise laminated, fining-upward mud with occasional shell fragments. Large storm or typhoon deposits show typically sharp and partly erosional lower contacts and are composed of rippled, cross-laminated and graded sand without mud. The 2004 Indian Ocean tsunami left three different sedimentary facies, including (1) sand enriched in shell and shell debris, (2) cross-bedded sand, and (3) layers including mud and sand clasts. From this study, the most prominent difference between the storm and tsunami deposits offshore from Khao Lak area is the presence of terrestrial components, anthropogenic artefacts and mud in the latter.

Acknowledgements. The authors wish to thank the Phuket Marine Biological Center (PMBC) for supporting us with ship time of RV *Chakratong Tongyai* and RV *Boonlert Pasook* as well as with other facilities during field campaigns. This study was funded through Deutsche Forschungsgemeinschaft (DFG) grant SCHW 572/11, the National Research Council of Thailand (NRCT) and the DAAD (Deutscher Akademischer Austausch Dienst) fellowship provided to Daroonwan Sakuna-Schwartz for a PhD study at Kiel University.

References

Abrantes, F., Alt-Epping, U., Lebreiro, S., Voelker, A., and Schneider, R.: Sedimentological record of tsunamis on shallow-shelf areas, The case of the 1969 AD and 1755 AD tsunamis on the Portuguese Shelf off Lisbon, Mar. Geol., 249, 283–293, 2008.

Allison, M. A., Sheremet, A., Goñi, M. A., and Stone, G. W.: Storm layer deposition on the Mississippi-Atchafalaya subaqueous delta generated by Hurricane Lili in 2002, Cont. Shelf Res., 25, 2213–2232, 2005.

Bahlburg, H. and Weiss, R.: Sedimentology of the December 26, 2004, Sumatra tsunami deposits in eastern India (Tamil Nadu) and Kenya, Int. J. Earth Sci., 96, 1195–1209, 2007.

Bahr, A., Lamy, F., Arz, H., Kuhlmann, H., and Wefe, G.: Late glacial to Holocene climate and sedimentation history in the NW Black Sea, Mar. Geol., 214, 309–322, 2005.

NHESSD

2, 7225–7267, 2014

Best, A. I. and Gunn, D. E.: Calibration of marine sediment core loggers for quantitative acoustic impedance studies, Mar. Geol., 160, 137–146, 1999.
Blott, S. J. and Pye, K.: Gradistat, a grain-size distribution and statistics package for the analysis of unconsolidated sediments, Earth Surf. Proc. Land., 26, 1237–1248, 2001.
Bourrin, F., Friend, P. L., Amos, C. L., Manca, E., Ulses, C., Palanques, A., Durrieu de Madron, X., and Thompson, C. E. L.: Sediment dispersal from a typical Mediterranean flood, the Têt River, Gulf of Lions, Cont. Shelf Res., 28, 1895–1910, 2008.
Brill, D., Brückner, H., Jankaew, K., Kelletat, D., Scheffers, A., and Scheffers, S.: Potential predecessors of the 2004 Indian Ocean Tsunami – sedimentary evidence of extreme wave events at Ban Bang Sak, SW Thailand, Sediment. Geol., 239, 146–161, 2011.
Brill, D., Pint, A., Jankaew, K., Frenzel, P., Schwarzer, K., Vött, A., and Brückner, H.: Sediment transport and hydrodynamic parameters of tsunami waves recorded in offshore Geoarchives – a case study from Thailand, J. Coastal Res., 30, 922–941, doi:10.2112/JCOASTRES-D-13-00206.1, 2014a.
Brill, D., Jankaew, K., Neubauer, N. P., Kelletat, D., Scheffers, A., Vött, A., and Brückner, H.: Holocene coastal evolution of southwest Thailand – implications for the site-specific preservation of palaeotsunami deposits, Z. Geomorphol., 58, 273–303, doi:10.1127/0372-8854/2014/0132, 2014b.
Cantalamessa, G. and Celma, C. D.: Sedimentary features of tsunami backwash deposits in a shallow marine Miocene setting, Mejillones Peninsula, northern Chile, Sediment. Geol., 178, 259–273, 2005.
Chagué-Goff, C., Schneider, J. L., Goff, J. R., Dominey-Howes, D., and Strotz, L.: Expanding the proxy toolkit to help identify past events – lessons from the 2004 Indian Ocean Tsunami and the 2009 South Pacific Tsunami, Earth-Sci. Rev., 107, 107–122, doi:10.1016/j.earscirev.2011.03.007, 2011.
Chavanich, S., Siripong, A., Sojisuporn, P., and Menasaveta, P.: Impact of tsunami on the seafloor and corals in Thailand, Coral Reefs, 24, 535p., 2005.
Cheng, W. and Weiss, R.: On sediment extent and runup of tsunami waves, Earth Planet. Sc. Lett., 362, 305–309, 2013.
Choowong, M., Murakoshi, N., Hisada, K., Charusiri, P., Daorerk, V., Charoentitirat, T., Chutakositkanon, V., Jankaew, K., and Kanjanapayont, P.: Erosion and deposition by the 2004 Indian Ocean Tsunami in Phuket and Pang-nga Provinces, Thailand, J. Coastal Res., 23, 1270–1276, 2007.

NHESSD
2, 7225–7267, 2014

Choowong, M., Phantuwongraj, S., Charoentitirat, T., Chutakositkanon, V., Yumuang, S., and Charusiri, P.: Beach recovery after 2004 Indian Ocean Tsunami from Phang-nga, Thailand, Geomorphology, 104, 134–142, 2009.

Colin, C., Turpin, L., Bertaux, J., Desprairies, A., and Kissel, C.: Erosional history of the Himalayan and Burman ranges during the last two glacial–interglacial cycles, Earth Planet. Sc. Lett., 171, 647–660, 1999.

Crokett, J. S. and Nittrouer, C. A.: The sandy inner shelf as a repository for muddy sediment, an example from Northern California, Cont. Shelf Res., 24, 55–73, 2004.

Curran, K. J., Hill, P. S., and Milligan, T. G.: Fine-grained suspended sediment dynamics in the Eel River flood plume, Cont. Shelf Res., 22, 2537–2550, 2002.

Cutter Jr, G. R. and Diaz, R. J.: Biological alteration of physically structured flood deposits on the Eel margin, northern California, Cont. Shelf Res., 20, 235–253, 2000.

Dartnell, P. and Gardner, J. V.: Predicting seafloor facies from multibeam bathymetry and backscatter data, Photogramm. Eng. Rem. S., 70, 1081–1091, 2004.

Dawson, A. G. and Stewart, I.: Tsunami deposits in the geological record, Sediment. Geol., 200, 166–183, 2007.

Dawson, A. G., Shi, S., Dawson, S., Takahashis, T., and Shutos, N.: Coastal sedimentation associated with the June 2nd and 3rd, 1994, tsunami in Rajegwesi, Java, Quaternary Sci. Rev., 15, 901–912, 1996.

Di Geronimo, I., Choowong, M., and Phantuwongraj, S.: Geomorphology and superficial bottom sediments of KhaoLak coastal area (SW Thailand), Pol. J. Environ. Stud., 18, 111–121, 2009.

Einsele, G., Ricken, W., and Seilacher, A. (Eds.): Cycles and Events in Stratigraphy, Springer-Verlag, Berlin, Heidelberg, New York, 955 pp., 1991.

Engel, M. and Brückner, H.: The identification of palaeo-tsunami deposits – a major challenge in coastal sedimentary research, Coastline Rep., 17, 65–80, 2011.

Feldens, P., Schwarzer, K., Szczuciński, W., Stattegger, K., Sakuna, D., and Somgpongchaiykul, P.: Impact of 2004 Tsunami on seafloor morphology and offshore sediments, Pakarang Cape, Thailand, Pol. J. Environ. Stud., 18, 63–68, 2009.

Feldens, P., Schwarzer, K., Sakuna, D., Szczuciński, W., and Somgpongchaiykul, P.: Identification of offshore tsunami deposits on the shelf off KhaoLak (Thailand), Earth Planets Space, 64, 875–887, 2012.

NHESSD
2, 7225–7267, 2014

Fujiwara, O. and Kamataki, T.: Identification of tsunami deposits considering the tsunami waveform, an example of subaqueous tsunami deposits in Holocene shallow bay on southern Bobo Penisular, Central Japan, Sediment. Geol., 200, 295–313, 2007.
Geyer, W. R., Hill, P. S., and Kineke, G. C.: The transport, transformation and dispersal of sediment by buoyant coastal flows, Cont. Shelf Res., 24, 927–949, 2004.
Goff, J., Chagué-Goff, C., and Nichol, S.: Paleotsunami deposits, a New Zealand perspective, Sediment. Geol., 143, 1–6, 2001.
Goff, J., McFadgen, B. G., and Chagué-Goff, C.: Sedimentary differences between the 2002 Easter storm and the 15th-century Okoropunga tsunami, southeastern North Island, New Zealand, Mar. Geol., 204, 235–250, 2004.
Goodman-Tchernov, B. N., Dey, H. W., Reinhard, E. G., McCoy, F., and Mart, Y.: Tsunami waves generated by the Santorini eruption reached Eastern Mediterranean shores, Geology, 37, 943–946, 2009.
Goto, K., Chavanich, S. A., Imamura, F., Kunthasap, P., Matsui, T., Minoura, K., Sugawara, D., and Yanagisawa, H.: Distribution, origin and transport process of boulders deposited by the 2004 Indian Ocean Tsunami at Pakarang Cape, Thailand, Sediment. Geol., 202, 821–837, 2007.
Goto, K., Takahashi, J., Oie, T., and Imamura, F.: Remarkable bathymetric change in the nearshore zone by the 2004 Indian Ocean Tsunami, Kirinda Harbor, Sri Lanka, Geomorphology, 127, 107–116, 2011.
Goto, K., Hashimoto, K., Sugawara, D., Yanagisawa, H., and Abe, T.: Spatial thickness variability of the 2011 Tohoku-oki tsunami deposits along the coastline of Sendai Bay, Mar. Geol., doi:10.1016/j.margeo.2013.12.015, in press, 2014.
Grzelak, K., Kotwicki, L., and Szczuciński, W.: Monitoring of sandy beach meiofaunal assemblages and sediments after the 2004 Tsunami in Thailand, Pol. J. Environ. Stud., 18, 43–51, 2009.
Harris, P. T. and Heap, A. D.: Cyclone-induced net sediment transport pathway on the continental shelf of tropical Australia inferred from reef talus deposits, Cont. Shelf Res., 29, 2011–2019, 2009.
Hill, P. S., Milligan, T. G., and Geyer, W. R.: Controls on effective settling velocity of suspended sediment in the Eel River flood plume, Cont. Shelf Res., 20, 2095–2111, 2000.
Hofmann, D. I., Fabian, K., Schneider, F., Donner, B., and Bleil, U.: A stratigraphic network across the Subtropical Front in the central South Atlantic, Multi-parameter correlation of mag-

NHESSD
2, 7225–7267, 2014

netic susceptibility, density, X-ray fluorescence and $\delta^{18}O$ records, Earth Planet. Sc. Lett., 240, 694–709, 2005.
Hylleberg, J., Nateewathana, A., and Chatananthawej, B.: Temporal changes in the macrobenthos on the west coast of Phuket Island, with emphasis on the effects of offshore tin mining, Phuket Mar. Biol. Cent. Res. Bull., 37, 1–16, 1985.
ICES: Sediment dynamics in relation to sediment trend monitoring, ICES Cooperative Research Report No. 308, International Council for the Exploration of the Sea, Copenhagen, Denmark, 34 pp., 2011.
Jankaew, K., Atwater, B. F., Sawai, Y., Choowong, M., Charoentitirat, T., Martin, M. E., and Prendergast, A.: Medieval forewarning of the 2004 Indian Ocean Tsunami in Thailand, Nature, 455, 1228–1231, 2008.
Kale, V. S.: Geomorphic effects of monsoon floods on Indian rivers, Nat. Hazards, 28, 65–84, 2003.
Khokiattiwong, S., Limpsaichol, P., Petpiroon, S., Sojisuporn, P., and Kjerfve, B.: Oceanographic variations in Phangnga Bay, Thailand under monsoonal effects, Phuket Mar. Biol. Cent. Res. Bull., 55, 43–76, 1991.
Kortekaas, S. and Dawson, A. G.: Distinguishing tsunami and storm deposits, an example from Martinhal, SW Portugal, Sediment. Geol., 200, 208–221, 2007.
Krumbein, W. C.: Size frequency distribution of sediments and the normal phi curve, J. Sediment. Petrol., 8, 84–90, 1938.
Kuehl, S. A., Nittrouer, C. A., Allison, M. A., Ercilio, L., Faria, C., Dukat, D. A., Jaeger, J. M., Pacioni, T. D., Figueiredo, A. G., and Underkoffler, E. C.: Sediment deposition, accumulation, and seabed dynamics in an energetic, fine-grained, coastal environment, Cont. Shelf Res., 16, 787–815, 1985.
Lamy, F., Hebbeln, D., Röhl, U., and Wefer, G.: Holocene rainfall variability in southern Chile, a marine record of latitudinal shifts of the Southern Westerlies, Earth Planet. Sc. Lett., 185, 369–382, 2001.
Lario, J., Luque, L., Zazo, C., Goy, J. L., Spencer, C., Cabero, A., Bardají, T., Borja, F., Dabrio, C. J., Civis, J., González-Delgado, J. A., Borja, C., and Alonso-Azcárate, J.: Tsunami vs. storm surge deposits, a review of the sedimentological and geomorphological records of extreme wave events (EWE) during the Holocene in the Gulf of Cadiz, Spain, Z. Geomorphol., 54, 301–316, 2010.

NHESSD
2, 7225–7267, 2014

Le Roux, J. P. and Vargas, G.: Hydraulic behavior of tsunami backflows, insights from their modern and ancient deposits, Environ. Geol., 49, 65–75, 2005.
Lorang, M. S.: A wave-competence approach to distinguish between boulder and megaclast deposits due to storm waves versus tsunamis, Mar. Geol., 283, 90–97, 2011.
Malmon, D. V., Reneau, S. L., and Dunne, T.: Sediment sorting and transport by flash floods, J. Geophys. Res.-Earth, 109, 1–13, 2004.
Martin, A. J.: Flaser and wavy bedding in ephemeral streams, a modern and an ancient example, Sediment. Geol., 136, 1–5, 2000.
McKee, B. A., Nittrouer, C. A., and DeMaster, D. J.: The concepts of sediment deposition and accumulation applied to the continental shelf near the mouth of the Yangtze River, Geology, 11, 631–633, 1983.
Milker, Y., Wilken, M., Schumann, J., Sakuna, D., Feldens, P., Schwarzer, K., and Schmiedl, G.: Sediment transport on the inner shelf off Khao Lak (Andaman Sea, Thailand) during the 2004 Indian Ocean Tsunami and former storm events: evidence from foraminiferal transfer functions, Nat. Hazards Earth Syst. Sci., 13, 3113–3128, doi:10.5194/nhess-13-3113-2013, 2013.
Milkert, D.: Auswirkungen von Stürmen auf die Schlicksedimente der westlichen Ostsee, Ber.-Rep., Geol.-Paläont. Inst., Univ. Kiel, Kiel, 66, 153 pp., 1995.
Morton, R. A., Gelfenbaum, G., and Jaffe, B. E.: Physical criteria for distinguishing sandy tsunami and storm deposits using modern examples, Sediment. Geol., 200, 184–207, 2007.
Mulder, T., Syvitski, J. P. M., Migeon, S., Faugères, J. C., and Savoye, B.: Marine hyperpycnal flows: initiation, behavior and related deposits: a review, Mar. Petrol. Geol., 20, 861–882, 2003.
Nanayama, F. and Shigeno, K.: Inflow and outflow facies from the 1993 tsunami in southwest Hokkaido, Sediment. Geol., 187, 139–158, 2006.
Nanayama, F., Shigeno, K., Satake, K., Shimokaka, K., Koitabashi, S., Miyasaka, S., and Ishii, M.: Sedimentary differences between the 1993 Hokkaido-nansei-oki tsunami and the 1959 Miyakojima typhoon at Taisei, southwestern Hokkaido, northern Japan, Sediment. Geol., 13, 255–264, 2000.
Nott, J. F.: Waves, boulders and the importance of the pre-transport setting, Earth Planet. Sc. Lett., 210, 269–276, 2003.

NHESSD
2, 7225–7267, 2014

Ogston, A. S., Cacchione, D. A., Sternberg, R. W., and Kineke, G. C.: Observations of storm and river flood-driven sediment transport on the northern California continental shelf, Cont. Shelf Res., 20, 2141–2162, 2000.
Ohta, T. and Arai, H.: Statistical empirical index of chemical weathering in igneous rocks, a new tool for evaluating the degree of weathering, Chem. Geol., 240, 280–297, 2007.
Owen, R. B. and Lee, R.: Human impacts on organic matter sedimentation in a proximal shelf setting, Hong Kong, Cont. Shelf Res., 24, 583–602, 2004.
Palinkas, C. M., Nittrouer, C. A., and Walsh, J. P.: Inner shelf sedimentation in the Gulf of Papua, New Guinea, a mud-rich shallow shelf setting, J. Coastal Res., 22, 760–772, 2006.
Paris, R., Fournier, J., Poizot, E., Etienne, S., Mortin, J., Lavigne, F., and Wassmer, P.: Boulder and fine sediment transport and deposition by the 2004 tsunami in LhokNga (western Banda Aceh, Sumatra, Indonesia), a coupled offshore-onshore model, Mar. Geol., 268, 43–54, 2010.
Phantuwongraj, S. and Choowong, M.: Tsunamis versus storm deposits from Thailand, Nat. Hazards, 63, 31–50, 2012.
Postma, G.: Physical climate signatures in shallow- and deep-water deltas, Global Planet. Change, 28, 93–106, 2001.
Ramaswamy, V., Rao, P. S., Rao, K. K., Swe Thwin, Rao, N. S., and Raiker, V.: Tidal influence on suspended sedimen distribution and dispersal in the northern Andaman Sea and Gulf Martaban, Mar. Geol., 208, 33–42, 2004.
Ramírez-Herrera, M.-T., Lagos, M., Hutchinson, I., Kostoglodov, V., Machain, M. L., Caballero, M., Goguitchaichvili, A., Aguilar, B., Chagué-Goff, C., Goff, J., Ruiz-Fernández, A.-C., Ortiz, M., Nava, H., Bautista, F., Lopez, G. I., and Quintana, P.: Extreme wave deposits on the Pacific coast of Mexico, tsunamis or storms? – a multi-proxy approach, Geomorphology, 139–140, 360–371, 2012.
Richmond, B. M., Watt, S., Buckley, M., Jaffe, B. E., Gelfenbaum, G., and Morton, R. A.: Recentstorm and tsunami coarse-clast deposit characteristics, southeast Hawaii, Mar. Geol., 283, 79–89, 2011.
Robbins, J. A. and Edgington, D. N.: Determination of recent sedimentation rates in Lake Michigan using Pb-210 and Cs-137, Geochim. Cosmochim. Acta, 39, 285–304, 19775.
Rodolfo, K. S.: Bathymetry and marine geology of the Andaman Basin, and tectonic implications for Southeast Asia, Geol. Soc. Am. Bull., 80, 1203–1230, 1969.

NHESSD
2, 7225–7267, 2014

Rose, L. E. and Kuehl, S. A.: Recent sedimentation patterns and facies distribution on the Poverty Shelf, New Zealand, Mar. Geol., 270, 160–174, 2010.
Sakuna, D., Szczuciński, W., Feldens, P., Schwarzer, K., and Khokiattiwong, S.: Sedimentary deposits left by the 2004 Indian Ocean Tsunami on the inner continental shelf offshore of KhaoLak, Andaman Sea (Thailand), Earth Planets Space, 64, 931–943, 2012.
Schwab, J. M., Krastel, S., Grün, M., Gross, F., Pananont, P., Jintasaeranee, P., Bunsomboonsakul, S., Weinrebe, W., and Winkelmann, D.: Submarine mass wasting and associated tsunami risk offshore western Thailand, Andaman Sea, Indian Ocean, Nat. Hazards Earth Syst. Sci., 12, 2609–2630, doi:10.5194/nhess-12-2609-2012, 2012.
Shanmugam, G.: Process-sedimentological challenges in distinguishing paleo-tsunami deposits, Nat. Hazards, 63, 5–30, doi:10.1007/s11069-011-9766-z, 2011.
Singh, O. P., Ali Khan, T. M., and Rahman, M. S.: Changes in the frequency of tropical cyclones over the North Indian Ocean, Meteorol. Atmos. Phys., 75, 11–20, 2000.
Siripong, A.: Andaman Sea coast of Thailand field survey after the December 2004 Indian Ocean Tsunami, Earthq. Spectra, 22, 187–202, 2006.
Smedile, A., De Martini, P. M., Pantosti, D., Bellucci, L., Del Carlo, P., Gasperini, L., Pirrotta, C., Polonia, A., and Boschi, E.: Possible tsunami signatures from an integrated study in the Augusta Bay offshore (Eastern Sicily-Italy), Mar. Geol., 281, 1–13, 2011.
Sommerfield, C. K. and Nittrouer, C. A.: Modern accumulation rates and sediment budget for the Eel shelf, a flood-dominated depositional environment, Mar. Geol., 154, 227–241, 1999.
Sommerfield, C. K., Drake, D. E., and Wheatcroft, R. A.: Shelf record of climatic changes in flood magnitude and frequency, north-coastal California, Geology, 30, 395–398, 2002.
Spiske, M., Piepenbreier, J., Benavente, C., and Bahlburg, H.: Preservation potential of tsunami deposits on arid siliciclastic coasts, Earth-Sci. Rev., 126, 58–73, 2013.
Spiske, M., Bahlburg, H., and Weiss, R.: Pliocene mass failure deposits mistaken as submarine tsunami backwash sediments – an example from Hornitos, Northern Chile, Sediment. Geol., 305, 69–82, doi:10.1016/j.sedgeo.2014.03.003, 2014.
Sugawara, D., Minoura, K., Nemoto, N., Tsukawaki, S., Goto, K., and Imamura, F.: Foraminiferal evidence of submarine sediment transport and deposition by backwash during the 2004 Indian Ocean Tsunami), Isl. Arc, 18, 513–525, 2009.
Switzer, A. D. and Jones, B. G.: Large-scale washover sedimentation in a freshwater lagoon from the southeast Australian coast, sea-level change, tsunami or exceptionally large storm?, Holocene, 18, 787–803, 2008.

NHESSD
2, 7225–7267, 2014

Szczuciński, W., Chaimanee, N., Niedzielski, P., Rachlewicz, G., Saisuttichai, D., Tepsuwan, T., Lorenc, S., and Siepak, J.: Environmental and geological impacts of the 26 December 2004 Tsunami in coastal zone of Thailand – overview of short and long-term effects, Pol. J. Environ. Stud., 15, 793–810, 2006.

Thai Meteorological Department (TMD): Tropical cyclones moving through Thailand during 63 years (1951–2013), available at: www.tmd.go.th/programs%5Cuploads%5Ccyclones%5CTC_track_63y_n.pdf (last access: 30 November 2014), 2014.

Thampanya, U., Vermaat, J. E., Sinsakul, S., and Panapitukkul, N.: Coastal erosion and mangrove progradation of Southern Thailand, Estuar. Coast. Shelf S., 68, 75–85, 2006.

Tipmanee, D., Deelaman, W., Pongpiachan, S., Schwarzer, K., and Sompongchaiyakul, P.: Using Polycyclic Aromatic Hydrocarbons (PAHs) as a chemical proxy to indicate Tsunami 2004 backwash in Khao Lak coastal area, Thailand, Nat. Hazards Earth Syst. Sci., 12, 1441–1451, doi:10.5194/nhess-12-1441-2012, 2012.

Tjallingii, R., Stattegger, K., Wetzel, A., and Phach, P. V.: Infilling and flooding of the Mekong River incised valley during deglacial sea-level rise, Quaternary Sci. Rev., 29, 1432–1444, 2010.

Typhoon Havens Handbook: Tropical cyclones affecting Phuket, available at: http://www.nrlmry.navy.mil/port_studies/thh-nc/thailand/phuket/text/frame.htm, last access: 22 November 2014.

Uchida, J. I., Fujiwara, O., Hasegawa, S., and Kamataki, T.: Sources and depositional processes of tsunami deposits, analysis using foraminiferal tests and hydrodynamic verification, Isl. Arc, 19, 427–442, 2010.

Umitsu, M., Tanavud, C., and Patanakanog, B.: Effects of landforms on tsunami flow in the plains of Banda Aceh, Indonesia, and Nam Khem, Thailand, Mar. Geol., 242, 141–153, 2007.

Usiriprisan, C., Chiemchindaratana, S., Shoosuwan, S., and Chatrapakpong, Y.: Offshore exploration for tin and heavy minerals in the Andaman Sea, Department of Mineral Resources, Bangkok, UNDP, New York, 224 pp., 1987.

van den Bergh, G. D., Boer, W., de Haas, H., van Weering, T. C. E., and van Wijhe, R.: Shallow marine tsunami deposits in Teluk Banten (NW Java, Indonesia), generated by the 1883 Krakatau eruption, Mar. Geol., 197, 13–34, 2003.

NHESSD
2, 7225–7267, 2014

Weber, M. E., Niessen, F., Kuhn, G., and Wiedicke, M.: Calibration and application of marine sedimentary physical properties using a multi-sensor core logger, Mar. Geol., 136, 151–172, 1997.

Weidong, D., Baoguo, Y., and Xiaogen, W.: Studies of storm deposits in China, a review, Cont. Shelf Res., 17, 1645–1658, 1997.

Weiss, R.: Sediment grains moved by passing tsunami waves, tsunami deposits in deep water, Mar. Geol., 250, 251–257, 2008.

Weiss, R. and Bahlburg, B.: A note on the preservation of offshore tsunami deposits, J. Sediment. Res., 76, 1267–1273, 2006.

Wheatcroft, R. A. and Drake, D. E.: Post-depositional alteration and preservation of sedimentary event layers on continental margins, I. The role of episodic sedimentation, Mar. Geol., 199, 123–137, 2003.

Wolanski, E. and Spagnol, S.: Environmental degradation by mud in tropical estuaries, Reg. Environ. Change, 1, 152–162, 2000.

Wright, L. D. and Nittrouer, C. A.: Dispersal of river sediments in coastal seas, six contrasting cases, Estuaries, 18, 494–508, 1995.

NHESSD

2, 7225–7267, 2014

Table 1. History of nine tropical storms and typhoons that approached within a 180-nautical-mile radius of Phuket during the 52-year period (1945–1996). Modified from the Typhoon Havens Handbook (2014).

Storm	Date	Maximum wind speed at storm centre (knots)
Harriet	26 Oct 1962	30
Lucy	1 Dec 1962	20
Gloria	21 Dec 1965	30
Sally	5 Dec 1972	40
Sarah	12 Nov 1973	25
Gay	4 Nov 1989	100
Forrest	15 Nov 1992	55
Manny	16 Dec 1993	20
Ernie	18 Nov 1996	22

NHESSD
2, 7225–7267, 2014

Table 2. List of the analysed sediment cores.

Core no.	Sampling year	Latitude (N)	Longitude (E)	Water depth (m)	Core recovery (cm)	Distance offshore (km)
051207-31	2007	08°47.176′	98°11.724′	15.9	70	7.2
030310-C2	2010	08°36.474′	98°12.454′	11.5	23	3.3
030310-C3	2010	08°38.708′	98°12.931′	9.5	97	3.2
030310-C7	2010	08°41.053′	98°12.763′	11.9	65	2.9
050310-C2	2010	08°45.438′	98°13.186′	9.8	75	4.1
050310-C4	2010	08°46.659′	98°12.269′	15.3	55	6.3

NHESSD
2, 7225–7267, 2014

Table 3. Characteristics of the sedimentary deposit in shallow water and their event interpretation.

Core no.	Photo	X-ray image	Section depth (cm)	Type of sedimentary contact	Sediment description	Identified event
030310-C3 (a-I)	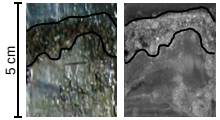 5 cm		29–34	upper: sharp lower: erosional	Top: a 2 cm thick layer of shell debris sand Bottom: laminated mud with mud clasts	Tsunami (2004) Top: facies A Bottom: facies B
(a-II)	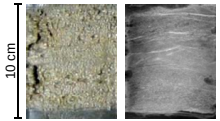 10 cm		47–57	upper: erosional lower: erosional	Massive sand layer with clear cross lamination that is observed in the upper 5 cm	Typhoon Gay (1989)
(a-III)	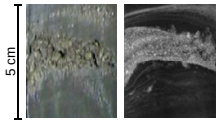 5 cm		66–71	upper: transitional (due to smearing) lower: sharp	Massive sand layer	Tropical storm (1972–1973)
(a-IV)	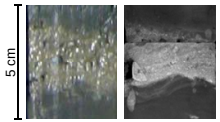 5 cm		78–83	upper: sharp lower: erosional	Massive sand layer including few shells	Tropical storm (1962–1965)
(a-V)	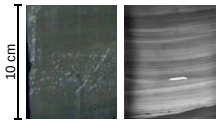 10 cm		85–95	upper: erosional lower: erosional	Fining-upward sequence laminated mud with no bioturbation	Flash flood (monsoon)
030310-C2 (b-I)	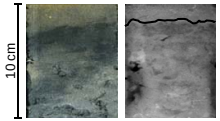 10 cm		3–13	upper: sharp lower: erosional	Homogenous fine sand	Tsunami facies C (2004)
(b-II)	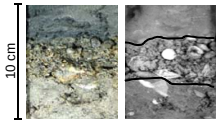 10 cm		10–20	upper: erosional lower: erosional	A 4 cm thick layer of shell fragments with admixture of gravels, laterites, corals and sand	Tsunami facies A (2004)

NHESSD
2, 7225–7267, 2014

Table 3. Continued.

Core no.	Photo	X-ray image	Section depth (cm)	Type of sedimentary contact	Sediment description	Identified event
050310-C4 (c-I)	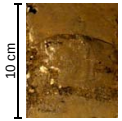		6–16	upper: sharp lower: erosional	Massive sandy mud with shell fragments scatter through the layer and laminated mud	Tsunami facies C (2004)
(c-II)	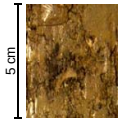		19–24	upper: erosional lower: erosional	Shell deposit in admixture of gravels, laterites and mud	Tsunami facies A (2004)
(c-III)	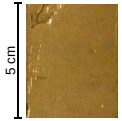		33–38	upper: sharp lower: sharp	Laminated fine-grained sediment	Flash flood (monsoon)
(c-IV)	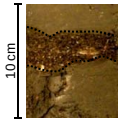	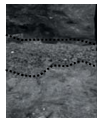	47–52	upper: erosional lower: sharp	Massive coarse sand layer	Typhoon Gay (1989)
030310-C7 (d-I)	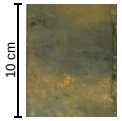	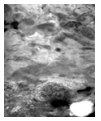	9–19	upper: transitional (due to bioturbation) lower: transional	Massive sediment that contains sandy and mud clasts scatter throughout the layer	Tsunami facies C (2004)
(d-II)	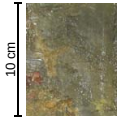	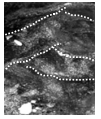	20–30	upper: transitional lower: transitional	Mud, sand and gravel partly cross laminated with generally fining upward grain size	Tsunami facies B (2004)
(d-III)	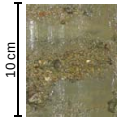	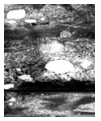	32–42	upper: transitional lower: sharp	A layer comprising coarse sand shell fragments, partly pebble-sized corals and pebbles	Tsunami facies A (2004)

NHESSD
2, 7225–7267, 2014

Table 3. Continued.

Core no.	Photo	X-ray image	Section depth (cm)	Type of sedimentary contact	Sediment description	Identified event
030310-C7 (cont.) (d-IV)	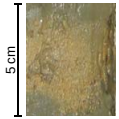	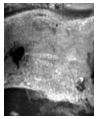	42–47	upper: sharp lower: sharp	Massive sand	Tropical storm (1992–1996)
(d-V)	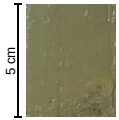	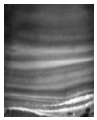	48–53	upper: sharp lower: sharp	Laminated mud, fining-upward sequences and no bioturbation	Flash flood (monsoon)
(d-VI)	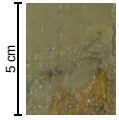	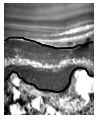	51–56	upper: sharp lower: sharp	Layers of draped mud	Resuspension
(d-VII)	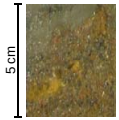	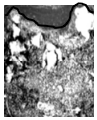	54–59	upper: sharp lower: sharp	Coarse sand and occasional pebbles	Typhoon Gay (1989)
051207-31 (e-I)	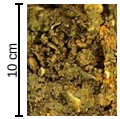	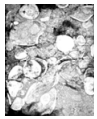	1–11	lower: erosional	Layer of shell deposits	Tsunami facies A (2004)
(e-II)	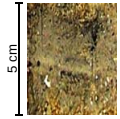	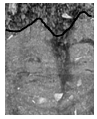	41–46	upper: sharp lower: sharp	Coarse-grained sediment with fining-upward sequence	Resuspension
(e-III)	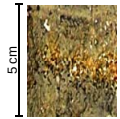	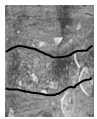	44–49	upper: sharp lower: sharp	Mixture of coarse sand and shell fragments	Tropical storm

NHESSD
2, 7225–7267, 2014

Table 3. Continued.

Core no.	Photo	X-ray image	Section depth (cm)	Type of sedimentary contact	Sediment description	Identified event
051207-31 (cont.) (e-IV)	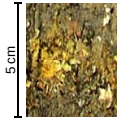 5 cm	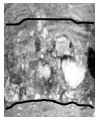	49–54	upper: sharp lower: erosional	Coarse sand with shell fragments	Tropical storm
(e-V)	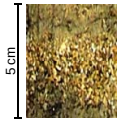 5 cm	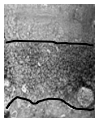	57–62	upper: sharp lower: erosional	Massive coarse sand	Tropical storm
(e-VI)	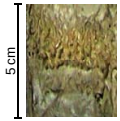 5 cm	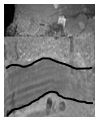	65–70	upper: transitional	Laminated fine-grained material	Flash flood
050310-C2 (f-I)	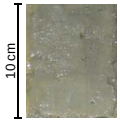 10 cm		12–22	upper: sharp lower: sharp	Laminate mud. No bioturbation traces exists	Resuspension
(f-II)	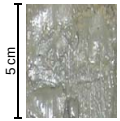 5 cm	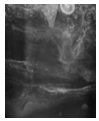	25–30	upper: sharp lower: erosional	Laminate mud. No bioturbation traces exists	Resuspension
(f-III)	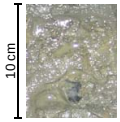 10 cm		30–40	upper: erosional lower: erosional	Shell deposit in sandy matrix	Tsunami facies A (2004)

NHESSD
2, 7225–7267, 2014

Table 4. Tsunami facies types.

Tsunami deposits facies types	X-ray images	Core no.	Section depth (cm)	Sediment description
A: sand enriched with shells or shell debris		051207-31	−10	A 10 cm thick of shell deposit at the top of core with a lower erosional contact
		030310-C2	10–20	A 4 cm thick layer of shell fragments with admixture of gravels, laterites, corals and sand
		030310-C3	29–34	A 2 cm thick layer of shell debris sand with sharp boundary at the top and bottom layer
		050310-C2	30–40	Shell deposit in sandy maxtrix with a sharp upper and lower boundary
		050310-C4	18.5–24	Shell deposit in admixture of gravels, laterites and mud
B: cross lamination	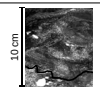	030310-C7	20–30	Mud, sand and gravel partly cross laminated with generally fining upward grain size
C: massive layers common with mud or sand clasts		030310-C2	3–13	Homogenous fine sand with an irregular sharp contact
		030310-C3	29–34	Laminated mud with mud clasts
		030310-C7	2–12	Homogenous mud with several mud clasts
		050310-C4	6–16	Massive mud with shell fragments scatter through the layer and mud clast

NHESSD
2, 7225–7267, 2014

Table 5. Differences between the sedimentary features of flash flood, tsunami and storm deposits on the Andaman Sea shelf.

Deposition characteristics	Flash flood (monsoon effect)	Tsunami	Tropical storm
Age of events (AD)	–	2004	1962–1965, 1972–1973, 1989
Occurrence (max. water depth)	16 m	16 m	45 m
Deposit thickness	1–12 cm	12–30 cm	2–9 cm
Sedimentary contact	transitional	sharp, erosional	sharp, erosional
Grain size range	mud	mud to gravels	silt to coarse sand
Sediment sorting	poorly sorted but better than tsunami deposits	poorly sorted	poorly sorted but better than tsunami deposits
Sedimentary structure	laminated, fining-upward sequences	laminated, massive structures, fining-upward sequence, internal erosional surfaces	rippled, cross-laminated, graded sand
Presence of rip-up clast	no	yes	no
Terrigenous component	no	wood and laterites	no
Anthropogenic artefact	no	pieces of brick	no
Presence of carbonate material	occasionally shell fragments	pieces of broken shells and corals	complete shells and their fragments (typical for beach sand)
Presence of mud	yes	yes	no
Presence of sand	no	yes	yes

NHESSD
2, 7225–7267, 2014

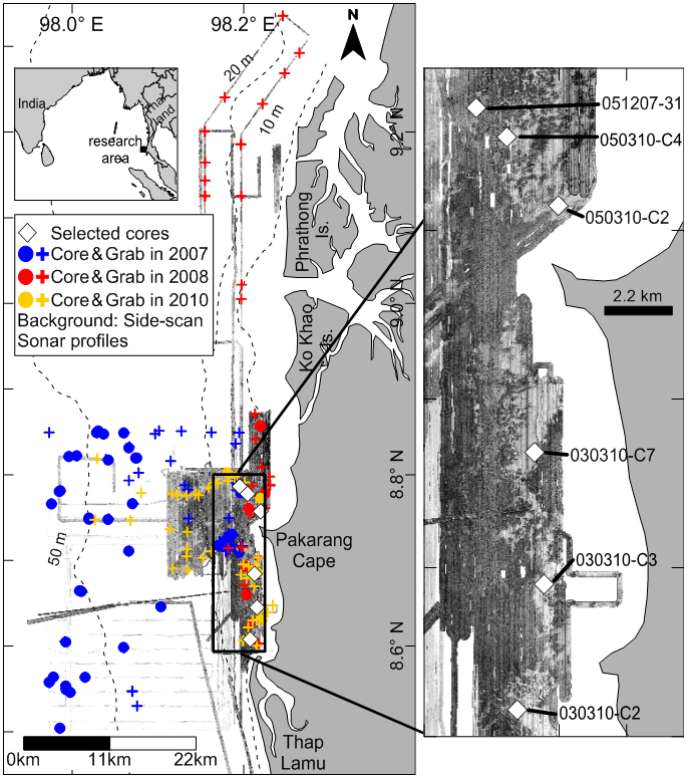

Figure 1. Overview map of the investigation area including sampling stations. The bathymetric data are based on nautical charts. The sediment samples taken during the 3-year research period are ordered due to the three different cruises in difference colours.

NHESSD
2, 7225–7267, 2014

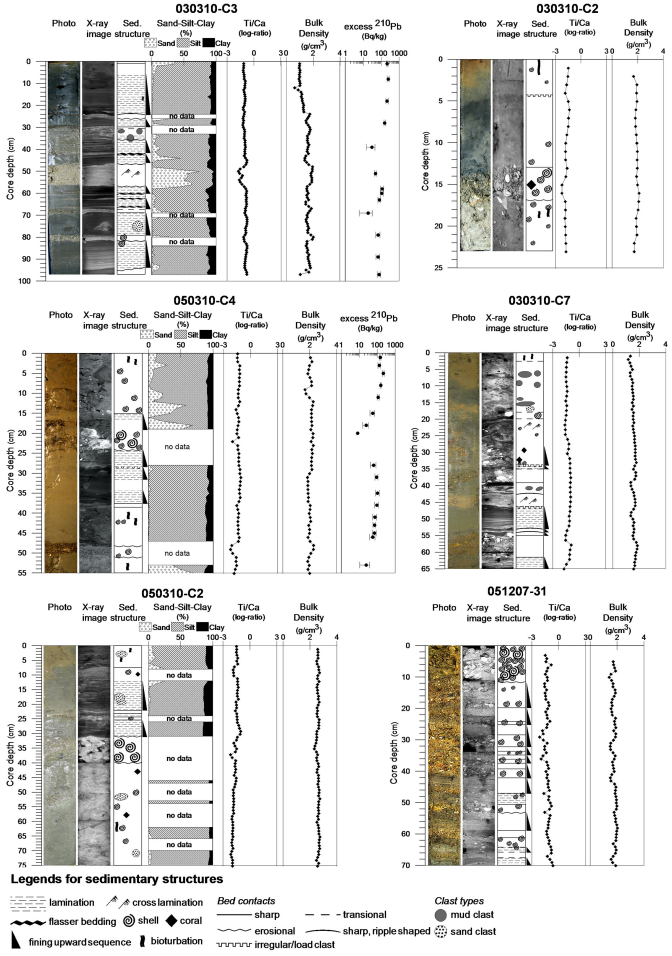

Figure 2. Interpretation of the sediment cores.

NHESSD
2, 7225–7267, 2014

Internal structure of event layers preserved on the Andaman Sea

D. Sakuna-Schwartz et al.

CC BY

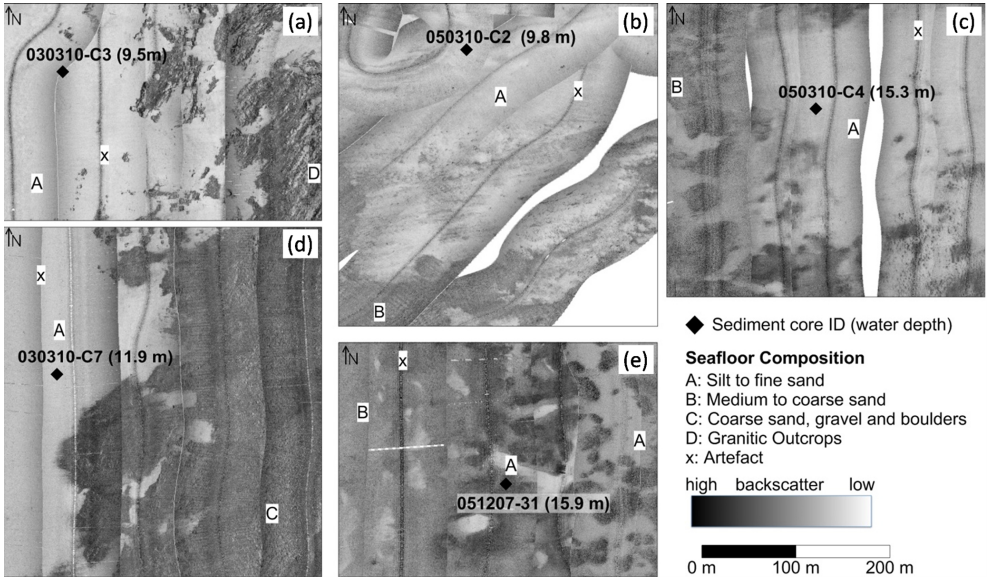

Figure 3. Cut-outs of the side-scan sonar mosaic showing the sediment distribution at the coring positions. No data are available for core 030310-C2. The composition of the seafloor was established based on the ground truthing of the backscatter data with grab samples and underwater video images (Feldens et al., 2012).

NHESSD
2, 7225–7267, 2014

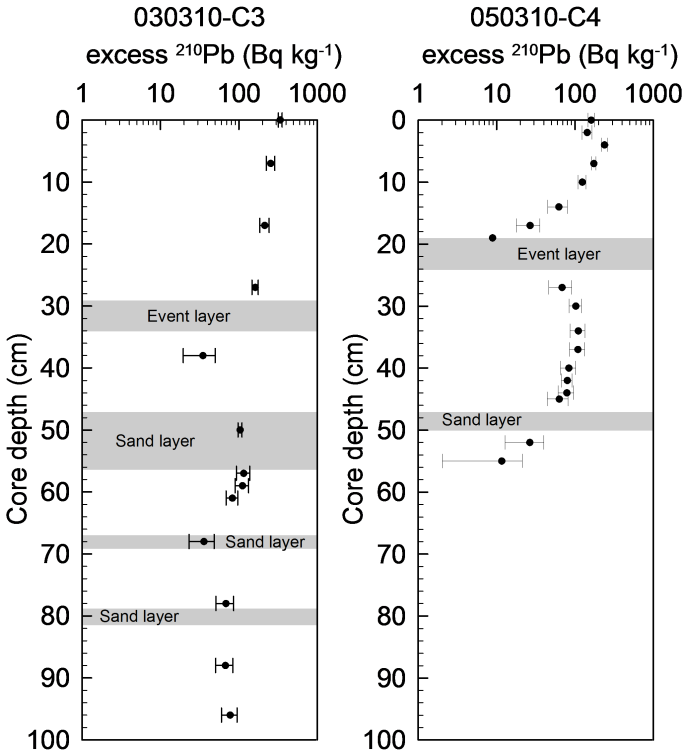

Figure 4. Excess ^{210}Pb activity profiles after mud correction with 2σ uncertainty ranges observed in the shallow water cores 030310-C3 and 050310-C4.

NHESSD
2, 7225–7267, 2014

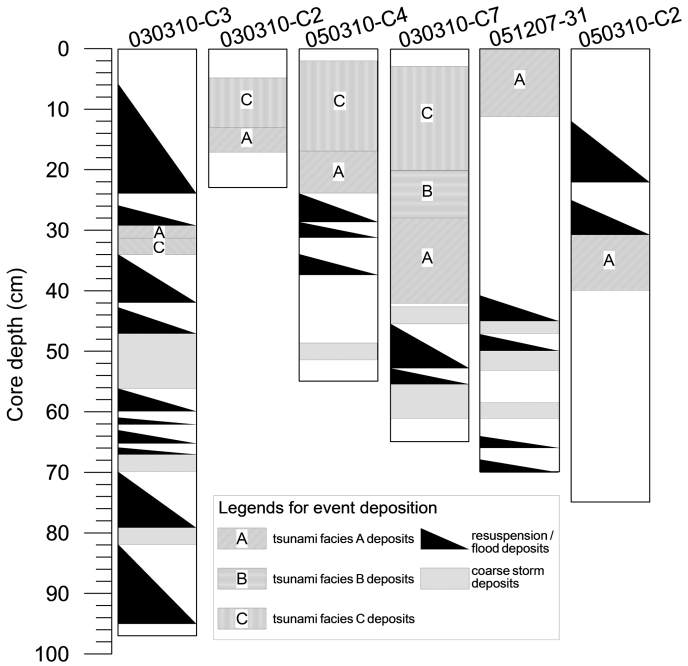

Figure 5. Event sequence log diagram for sediment cores taken in shallow water (< 16 m water depth).

NHESSD
2, 7225–7267, 2014

Internal structure of event layers preserved on the Andaman Sea

D. Sakuna-Schwartz et al.

CC BY